https://doi.org/10.5194/essd-2025-646
Preprint. Discussion started: 3 February 2026

Open Access Earth System Science Data Discussions

A Global Drought Dataset from Clustering-Based Event Identification with Integrated Population, and GDP Exposure and Socioeconomic Impacts

Alok Kumar Samantaray[1,2], Gabriele Messori[1,2]

1. Department of Earth Sciences, Uppsala University, Uppsala, 75236, Sweden
2. Swedish Centre for Impacts of Climate Extremes (climes), Sweden
Correspondence to: Alok Kumar Samantaray (alok.samantaray@geo.uu.se)

Abstract

Drought events pose significant challenges to both ecosystems and human societies, requiring precise methodologies for their detection and impact assessment. A key challenge is linking physical drought indicators to socioeconomic consequences, such as the number of people affected or economic losses. This study introduces a robust two-step framework that integrates drought detection with impact analysis. In the first step, a clustering algorithm is used to identify coherent drought events and extract key characteristics such as severity and spatial extent. These events are tracked as spatially and temporally evolving objects. In the second step, the drought events are linked to population and GDP exposure, as well as to impact data from global disaster databases.

To characterize droughts, the study employs two widely used drought indices: the Standardized Precipitation Index (SPI) and the Standardized Precipitation Evapotranspiration Index (SPEI). Precipitation and temperature data from the ERA5 reanalysis are used to compute these indices at four different timescales (1, 3, 6, and 12 months). Drought events are identified for different severity levels (-1, -1.5, and -2). The study also incorporates high resolution gridded datasets of global population and economic activity, alongside disaster impact data on affected populations and economic losses. The resulting drought dataset provides valuable information on the association between drought characteristics, exposure, and recorded impacts.

The analysis shows that a relatively large buffer distance is needed to match the identified drought events to impacts from disaster databases, and that more severe drought thresholds isolate fewer but higher-impact events. Population exposure is found to be highest in Asia, while GDP exposure is largest in North America. This integrated framework (https://doi.org/10.5281/zenodo.17251815; Samantaray & Messori, 2025) bridges the gap between physical drought characteristics, exposure, and documented impacts, supporting vulnerability analyses, improved climate adaptation planning and disaster risk management.

Keywords: Drought Analysis, Socioeconomic Impacts, Drought Clustering, EM-DAT, GDIS

https://doi.org/10.5194/essd-2025-646
Preprint. Discussion started: 3 February 2026

1) Introduction

Drought is a complex natural hazard that poses considerable challenges for accurate monitoring and effective management (Wilhite, 2016). Unlike storms, temperature extremes or floods, drought conditions often develop gradually and go unnoticed in their early stages, rather than presenting a distinct onset (Mishra & Singh, 2010; Mishra & Singh, 2011). This creeping nature makes drought challenging to detect and monitor in a timely manner; however, understanding its key characteristics such as severity and duration is crucial for effective planning and risk mitigation (Tsakiris et al., 2007). Drought can be classified into several types, which are identified using different hydroclimatic variables (Mishra & Singh, 2010). For example, precipitation deficits are used to identify meteorological drought, streamflow deficits to identify hydrological drought, and low soil moisture or groundwater to identify agricultural drought. This study focuses on meteorological drought.

To monitor and quantify meteorological droughts systematically, researchers often rely on drought indices (Zargar et al., 2011) such as the Standardized Precipitation Index (SPI; McKee et al., 1993) and the Standardized Precipitation Evapotranspiration Index (SPEI; Vicente-Serrano et al., 2010). These indices provide consistent, objective measures of anomalies over various temporal scales and serve as the foundation for assessing drought characteristics. One widely used approach for characterizing droughts based on these indices is statistical run theory, which defines drought events as periods during which hydrological variables remain below predefined thresholds for consecutive time steps (Yevjevich, 1967). Within this framework, drought severity is quantified by the cumulative water deficit over the duration of the event, enabling precise identification of drought onset, persistence, and recovery phases (Zhang, 2024).

Globally, droughts between 1998 and 2017 caused economic losses totalling approximately USD $124 billion, demonstrating the vast scale of drought impacts (UNCCD, 2023). Over recent years, drought events characterized by exceptional severity and prolonged durations have been observed globally, significantly impacting the environment, economy, and society (Buras et al., 2020; Pokhrel et al., 2021; Vicente-Serrano et al., 2022; Samantaray et al., 2022). For instance, the 2014-2015 drought event in India affected around 330 million people, resulting in extreme water scarcity and widespread agricultural losses, highlighting the region's vulnerability (Kafle et al., 2022). South America, notably the Amazon basin, faced severe drought conditions from 2022 to 2024, influenced by oceanic anomalies associated with El Niño events. This prolonged drought led to historically low river levels, disrupted transportation, and increased wildfire frequency, profoundly altering the region's ecosystem (Marengo et al., 2024). Europe also experienced severe drought conditions in 2022, primarily caused by significant soil moisture deficits and low river discharges, exacerbated by anthropogenic climate change. This event caused major agricultural losses, hydropower reductions, and interruptions to river navigation (Bevacqua et al., 2024). Droughts also trigger human migration, notably in Africa. Populations often move toward rivers and urban areas in search of water and economic opportunities during drought periods, illustrating a clear link between drought severity and human displacement (Ceola et al., 2023). Additionally, climate models predict increased drought severity and frequency in several regions, including South and North America (Penalba & Rivera, 2013; Cook et al., 2020; Samantaray et al., 2025).

https://doi.org/10.5194/essd-2025-646
Preprint. Discussion started: 3 February 2026

Recent studies have extensively used disaster databases, such as the Geocoded Disasters Dataset (GDIS; Rosvold & Buhaug, 2021) dataset, to examine drought-related socio-economic impacts at subnational scales. Kulkarni et al. (2024) evaluated multiple drought indices, including a novel Combined Drought Indicator (CDI), and confirmed their effectiveness in accurately identifying drought-affected regions and associated socioeconomic impacts. Similarly, Kageyama & Sawada (2024) used the GDIS dataset to investigate global drought events, emphasizing the relationship between drought severity and subsequent socio-economic consequences, such as agricultural losses, displacement, and economic disruptions. Such research underscores the critical importance of integrating comprehensive drought monitoring and assessment methodologies with information on drought impacts, to plan and mitigate socio-economic risks (Jägermeyr & Frieler, 2018; Marengo et al., 2022; Petersen-Perlman et al., 2022).

The above-discussed studies evidence that the impact of drought varies significantly across both space and time. The association between drought indices and impact data is thus both localized and temporally variable. This speaks to the need for analytical methods for identifying spatially coherent drought-affected regions and tracking the droughts' temporal evolution. Ghasempour et al. (2022) employed clustering techniques to regionalize drought areas based on satellite indices such as normalized difference vegetation index (NDVI). Kageyama & Sawada (2022) used the GDIS dataset coupled with ERA5-Land reanalysis data to demonstrate how drought hazards translate into socio-economic impacts at subnational levels, emphasizing the value of precise local-scale data. Herrera-Estrada et al. (2017) used a Lagrangian approach to monitor drought clusters' temporal and spatial progression, viewing droughts as continuous spatiotemporal phenomena with complex propagation dynamics.

Understanding drought dynamics is critical, given their increasing frequency, severity, and widespread socio-economic impacts across the globe. Despite significant advancements, accurately identifying drought events and relating their characteristics to the associated impacts remains a challenge (AghaKouchak et al., 2023). Specifically, we lack a globally consistent framework that combines spatiotemporal drought clustering with high-resolution socioeconomic exposure and impact data. This study addresses this challenge by pursuing three primary objectives. First, it seeks to develop a robust clustering algorithm capable of systematically identifying distinct spatio-temporal drought "objects," enabling automated extraction of key drought characteristics such as severity and spatial extent. Second, the study aims to assign population and economic exposure to the physical drought information as identified through the clustering process. Third, the study relates drought characteristics to impact data from the Emergency Events database (EM-DAT, Guha-Sapir et al., 2023). The resulting dataset and the code used to generate it are made publicly available for research and policy development purposes.

2) Data

We utilise precipitation and temperature data from the ERA5 reanalysis (Hersbach et al., 2023) provided by the European Centre for Medium-Range Weather Forecasts (ECMWF). The data has a horizontal resolution of 0.25° and we analyse the period from 1960 to 2018. To facilitate drought index calculation, the daily data are aggregated to a monthly timescale. These climate variables serve as the basis for computing the SPI and the SPEI drought indices at multiple timescales.

https://doi.org/10.5194/essd-2025-646
Preprint. Discussion started: 3 February 2026

Open Access Earth System Science Data Discussions

We also employ socioeconomic impact data from EM-DAT (Guha-Sapir et al., 2023) and geographical locations from GDIS (Rosvold & Buhaug, 2021). EM-DAT offers quantitative, categorical information on disaster impacts, including the number of people affected and total economic losses. However, it reports disasters at country level and only indicates subnational locations in non-standardised textual form. GDIS provides georeferenced information for a subset of the disaster events reported in EM-DAT, covering the years 1960-2018, which constitute our study period, facilitating a spatially explicit linkage between drought events and their impacts. These impact data are integrated with the drought indices to examine the relationship between drought characteristics and socioeconomic outcomes, as elaborated in later sections. To illustrate the spatial heterogeneity of the drought events reported in GDIS, we have plotted them in Figure 1. China displays the highest frequency, reporting over 30 drought events during the study period. Other countries with a high number of reported events include the United States, Brazil, Argentina, Australia, and several nations in Southern and Eastern Africa, each with between 15 and 25 recorded droughts. In contrast, the northern latitudes, parts of Europe, and some equatorial regions exhibit relatively fewer drought reports, reflecting potential underreporting or lower drought occurrence.

To assess socioeconomic exposure to drought, two high-resolution gridded datasets are utilised. The first is a global Gross Domestic Product (GDP) dataset (rast_gdpTot_1990_2022_5arcmin.tif) obtained from Kummu et al. (2023), which provides estimates of total GDP in constant 2015 US dollars from 1990 to 2022 at a spatial resolution of 5 arcminutes (approximately 10 km at the equator). GDP values are spatially disaggregated using national GDP data combined with subnational economic proxies, offering a realistic depiction of economic exposure at local scales. The second is the World Settlement Footprint (WSF; Marconcini et al., 2020) population time series, obtained from the Copernicus Emergency Management Service (CEMS). It provides gridded population estimates at a high spatial resolution of 1 km, covering the period from 1975 to 2025 in 5-year intervals. The data is derived through a combination of remote sensing (e.g., Landsat-based settlement detection), census data, and modelling. The dataset is designed to reflect residential population distribution and is particularly suited for applications in disaster risk assessment and humanitarian response (Chen et al., 2024). For both the population and GDP datasets, we limit the analysis to 2018 to match the end-date of GDIS, but the study periods nonetheless differ as neither dataset is available from 1960.

https://doi.org/10.5194/essd-2025-646
Preprint. Discussion started: 3 February 2026

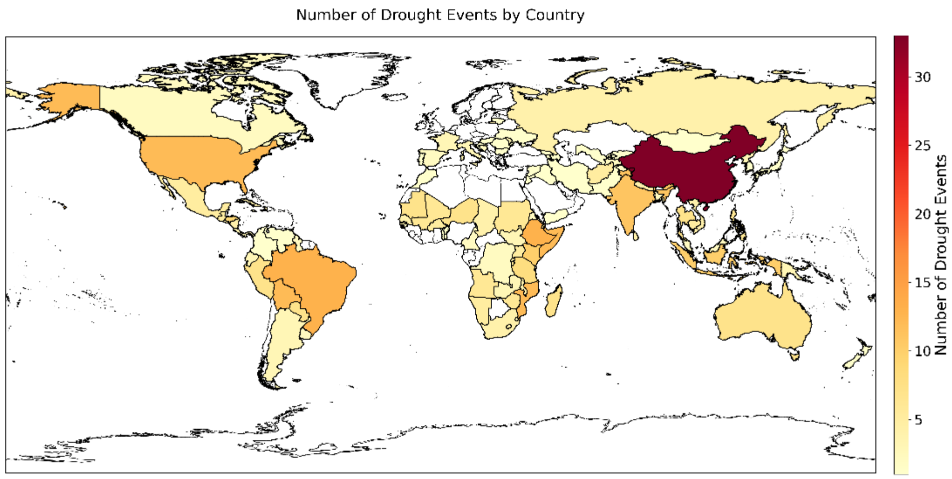

Figure 1. Global distribution of drought events reported in the GDIS dataset.

These datasets provide a comprehensive foundation for linking meteorological drought conditions to real-world socioeconomic consequences. The subsequent methodology section outlines the step-by-step process used to detect drought events, harmonize disaster records and quantify the exposure of both populations and economies to drought hazards.

3) Methodology

The methodology of this study is designed to establish a systematic link between physical drought indicators, population and GDP exposure, and socioeconomic impacts. First, a matching process is conducted between the EM-DAT and GDIS datasets. Second, the SPI and the SPEI are computed across multiple timescales and threshold values, and used to detect spatio-temporally coherent drought-affected regions. Finally, the drought data is connected to the population, GDP and impacts data.

3.1) Cross-Referencing Drought Events in EM-DAT and GDIS

While GDIS builds on EM-DAT, there are some geographic inconsistencies across the two sources, including in country names. The first step in resolving these inconsistencies is the development of a country correction dictionary, mapping former political entities to their respective modern successor states. Additionally, the dictionary includes mappings for countries that have undergone name changes in recent decades such as Swaziland to Eswatini and standardizes naming variants like “Bolivia (Plurinational State of)” and “United States of America” to their commonly used equivalents. This standardisation step is applied to both EM-DAT and GDIS. Following the textual harmonization of country names, a geospatial verification step is introduced to enhance the robustness of the matching process. Each drought event record is geolocated using a global shapefile of national boundaries. The geospatially derived country name is then compared against the standardized names from both GDIS and EM-DAT.

https://doi.org/10.5194/essd-2025-646
Preprint. Discussion started: 3 February 2026

Open Access Earth System Science Data Discussions

Table 1. Discrepancies in Reported Drought Event Locations Between GDIS and EM-DAT

Disasterno	Latitude	Longitude	GDIS	EM-DAT	Year	ISO3 GDIS
2014-9580	8,760251912	-63,87780838	Venezuela	Costa Rica, Nicaragua, El Salvador	2015	VEN
2012-9355	-6,81120164	-79,55017972	Peru	Guatemala	2012	PER
2014-9277	-6,81120164	-79,55017972	Peru	Guatemala	2014	PER
1997-9227	5,353369065	-6,675278369	Côte d'Ivoire	Nicaragua	1997	IVO
1999-9404	5,353369065	-6,675278369	Côte d'Ivoire	Paraguay	1999	IVO
2012-9021	5,353369065	-6,675278369	Côte d'Ivoire	Paraguay	2012	IVO
2013-9496	5,353369065	-6,675278369	Côte d'Ivoire	Paraguay	2013	IVO

One recurring issue is the presence of identical disaster numbers attributed to different countries across the two datasets. A notable example is disaster ID 2014-9580, which EM-DAT attributes to Costa Rica, Nicaragua, and El Salvador, while GDIS associates with Venezuela – a country not mentioned in the EM-DAT entry.

To resolve these discrepancies, a distance-threshold-based filtering approach is employed. Specifically, we measure the distance between the event coordinates recorded in GDIS and the centroid of the countries listed in EM-DAT. If this distance exceeds a predetermined threshold, the match is considered invalid. We tested several distance thresholds: 0 km, 100 km, 250 km, and 500 km to assess their impact on the number of mismatches. We found 9 mismatches at both 0 km and 100 km, and 7 at both 250 km and 500 km. Based on these results, we selected 250 km as a balanced threshold that accounts for potential regional reporting variations while maintaining geographic specificity. Accordingly, the seven discrepant events (Table 1) were excluded from further analysis.

3.2) Drought Indices

We identify droughts through two widely-used indices: SPI and SPEI. Both offer a flexible, multi-scalar framework to assess drought conditions across temporal and spatial domains. The SPI, developed by McKee et al. (1993), relies solely on precipitation data and evaluates deviations from the long-term mean over user-defined accumulation periods. It allows for direct comparisons of drought severity across diverse climates and regions. However, it does not incorporate temperature, and therefore may underestimate drought severity in warming climates where evaporative demand is rising (Zarch et al., 2015). To address this limitation, the SPEI, developed by Vicente-Serrano et al. (2010), integrates both precipitation and potential evapotranspiration (PET) to calculate a climatic water balance (precipitation minus PET). The inclusion of temperature effects makes SPEI more sensitive to climate change and

https://doi.org/10.5194/essd-2025-646
Preprint. Discussion started: 3 February 2026

better suited for detecting droughts driven by both precipitation deficits and increased atmospheric demand. In our analysis, we consider timescales of 1, 3, 6 and 12 months for both indices, and identify a gridpoint as being affected by drought using SPI and SPEI thresholds of -1, -1.5 and -2.

3.3) Spatio-Temporal Drought Event Identification

In GDIS, a single EM-DAT disaster number may correspond to multiple coordinates, which we refer to as target points. To detect spatiotemporal drought events, we begin by collecting all target points associated with each disaster number. We then calculate the distances between all pairs of target points to assess their geographic proximity and identify whether any points are distant from the rest. If a target point or set of target points has a nearest distance that exceeds a predefined maximum distance threshold (D_{max}) from any other target points, the algorithm divides the target points into separate groups. After forming these initial groups, geographic bounding boxes are constructed around them. To include surrounding areas that may also be affected by drought, the bounding boxes are expanded outward in all four cardinal directions using a spatial buffer distance (D_{buffer}) applied from the outermost coordinates of each group. The algorithm also allows for country-level analysis, instead of the bounding-box approach, by using country information from the same GDIS dataset. In this study, the bounding-box approach is applied, with D_{buffer} set to half the value of D_{max} to prevent overlap between different target point groups. However, the algorithm allows users to adjust these parameters based on their specific needs.

Within each bounding box, the methodology applies a threshold to the drought index values such as the SPI or SPEI to identify affected grid cells. Grid points that fall below the threshold are classified as drought-affected. A land-sea mask is applied to exclude ocean regions. We then identify spatially contiguous clusters of drought-affected grid points using connected component analysis based on eight-point connectivity. This method, commonly used in image processing, defines connectivity by considering all eight immediate neighbors of a pixel (including diagonal ones). Additionally, clusters for which the minimum distance between the two closest points in the clusters is less than a predefined merging distance (D_{merge}), are combined into single entities.

In addition to providing target points for each disaster number, GDIS also provides a single year of occurrence, referred to as the target year. For each GDIS disaster number, our algorithm returns all clusters that match the target points and target year. The algorithm is highly flexible and also provides the option to use the start year, start month, end year, and end month information from EM-DAT for the analysis. To help the reader better understand this workflow, a visual summary is provided in Figure 2. To illustrate the temporal evolution of drought clusters, we randomly selected a single drought event (disaster number: 2000-9860), and present its monthly progression over twelve consecutive months in Figure 3. Each sub-panel corresponds to a specific month, visualizing how the drought-affected region expands, contracts, and shifts spatially within Central America. In the early months (January to April), pronounced drought clusters are concentrated predominantly in the northern parts of Central America. As the year progresses (May to August), the clusters expand and shift toward southern regions. Toward the end of the year (September to December), the spatial distribution becomes more fragmented, with smaller and more isolated clusters. The monthly cluster

https://doi.org/10.5194/essd-2025-646
Preprint. Discussion started: 3 February 2026

Open Access Earth System Science Data Discussions

patterns demonstrate that drought conditions exhibit significant variability over short periods, influenced by climatic variability and other regional factors.

3.4) Connecting Drought Events to Exposure and Impact Data

We compute both population and GDP exposure for the drought clusters identified as matching drought events reported in GDIS, using the WSF population dataset and a gridded GDP dataset. To compute the exposure, we consider the population and GDP values across all pixels which lie in a drought cluster for at least one month during the target year. In addition to total exposure, this study employs a weighted exposure metric that accounts for both frequency and severity of drought at each pixel. Frequency weighting (WF) is defined as the number of months a pixel experiences drought divided by the total number of months in a year (12). Severity weighting (WS) is applied linearly on a continuous scale from 0 to 1, corresponding to average severity values ranging from 0 to -2. The maximum value of 1 is assigned to severity values ≤ -2 to avoid overestimation from locally extreme drought conditions. The combined weight is calculated as the product of WF and WS, following the widely accepted risk formulation: Risk = Frequency × Severity. Importantly, the algorithm also allows users to define and apply custom weighting schemes as needed. The results of both the total and weighted population exposure analyses are presented in the Results section.

We use impact data, specifically, the number of people affected and total economic losses, from the EM-DAT database to assess the consequences of drought events. Since our algorithm links drought clusters to GDIS event locations, it is sufficient to match each GDIS entry to its corresponding EM-DAT entry (see Sect. 3.1).

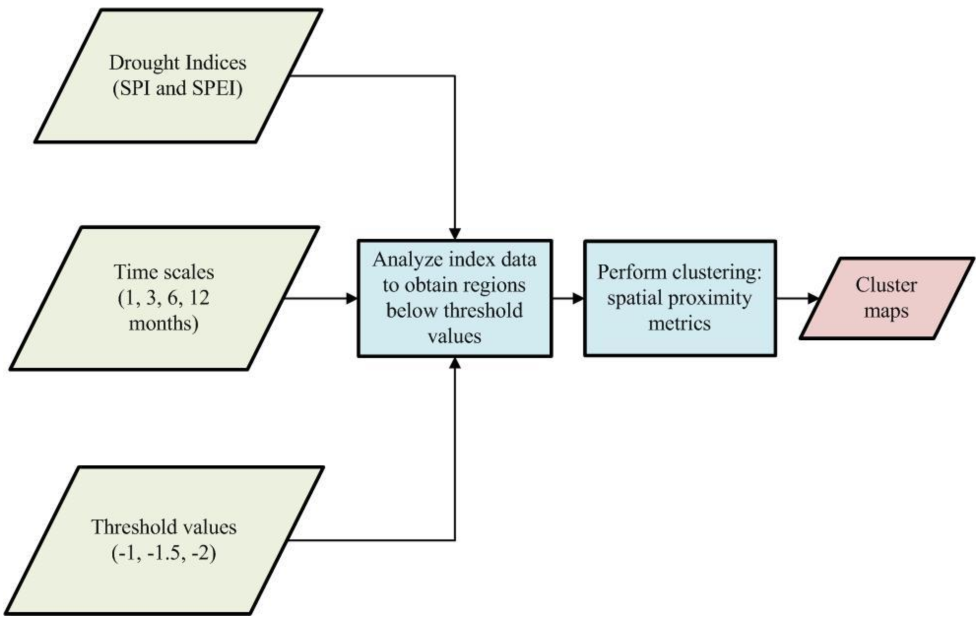

Figure 2. Flowchart summarizing the methodological framework for identifying drought clusters.

https://doi.org/10.5194/essd-2025-646
Preprint. Discussion started: 3 February 2026

Earth System Science Data
Open Access
Discussions

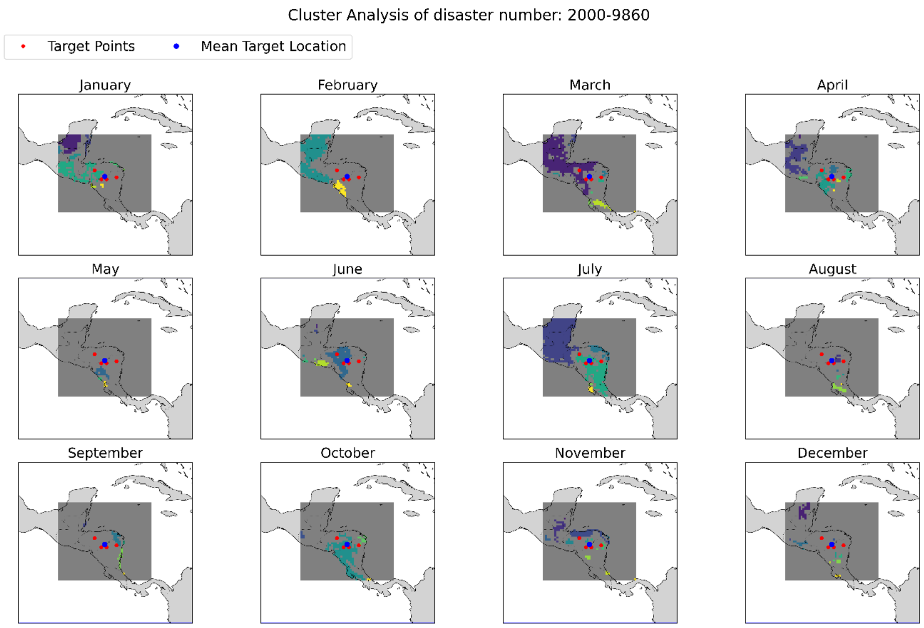

Figure 3. Spatial evolution of drought clusters over twelve consecutive months for a selected drought event (Disaster No. 2000-9860) in Central America. The bounding box is shown in dark grey. Different clusters are shown in different colours. The red dots (same in each panel) represent the original target points obtained from the GDIS dataset, while the blue dots indicate the mean location calculated from the target points, providing a representative geographic centroid.

4) Results

4.1) Matching Drought Events to Impact Data

We first investigate the percentage of drought events in the GDIS dataset for which one or more drought clusters are identified, as a function of the chosen SPI threshold (-1, -1.5, and -2), buffer distance (100 km, 250 km, and 500 km), and SPI timescale (1, 3, 6, and 12 months). Across all SPI timescales, higher detection percentages are generally associated with larger buffer distances and less severe event thresholds (Figure 4). The highest match percentages, often in the range of 90%, are observed when using a 500 km buffer distance and a -1 SPI threshold. These drop below 60% for more stringent parameter sets. This large variability highlights the importance of users selecting parameter combinations tailored to their specific applications. We evaluate the detection percentage again using SPEI data (Figure S1). The results remain similar to those of SPI. However, for any given threshold and timescale, the detection percentage is consistently higher with SPEI compared to SPI.

https://doi.org/10.5194/essd-2025-646
Preprint. Discussion started: 3 February 2026

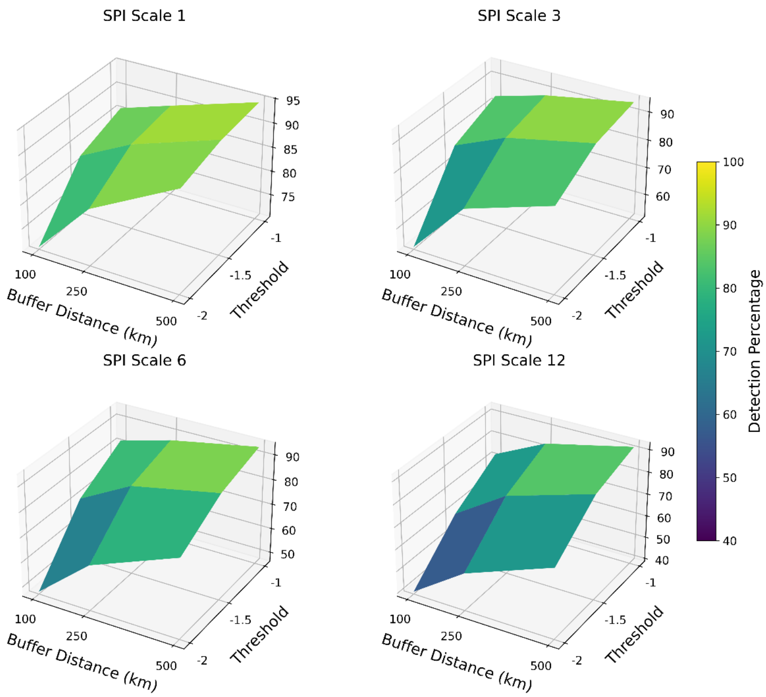

Figure 4. Percentage of drought events reported in the GDIS dataset which match one or more drought clusters for different SPI timescales (1, 3, 6, and 12 months), SPI threshold values (-1, -1.5, -2) and buffer distances (D_{buffer} = 100 km, 250 km, 500 km).

4.2) Population Exposure Based on Gridded Population Density

Figure 5 presents data across five continents: Asia, North America, Africa, South America, and Europe, at the SPI-1 (1-month) timescale. Australia is omitted due to the low number of reported events. Asia generally shows the highest population exposure across all drought time scales, except at lower thresholds, where Europe shows the highest exposure. Under a 500 km buffer distance and threshold -1, up to 0.6 billion people are exposed, primarily due to the region's dense population, as noted by Khan et al. (2018) and Mondal et al. (2021). Europe, North America and Africa follow, with approximately 150-750 million people exposed, while South America reports around 60 million under the same algorithm parameter set. As the drought severity threshold becomes more stringent, the areal extent of drought clusters declines across all continents, consistent with the severity–area relationship (Mishra & Singh, 2009; Kumar et al., 2021). Consequently, reduced drought area leads to lower population exposure.

https://doi.org/10.5194/essd-2025-646
Preprint. Discussion started: 3 February 2026

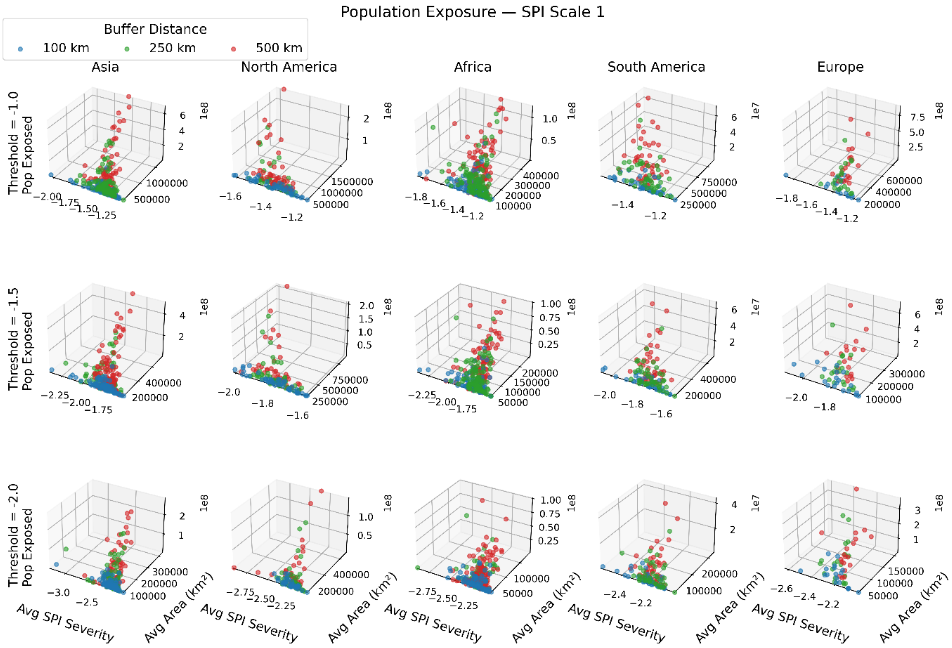

Figure 5. Population exposure to drought events based on SPI-1 (1-month timescale) across five continents: Asia, North America, Africa, South America and Europe using the WSF population dataset.

In terms of affected area, North America leads with up to 2 million km² at threshold -1, followed closely by Asia. South America, Europe, and Africa, with areas between 0.5 and 1 million km². At more severe thresholds, the same ranking holds, though the absolute differences shrink. This suggests that, for some large-area events at threshold -1, the majority of affected areas experience moderately severe drought conditions (see Figure 5). The most severe droughts (severity < -3) occur primarily in Asia, North America and Africa, while the most extreme events in other continents typically have severity around or slightly below -2.8. Overall, the relationships among drought severity and area at the SPI-1 scale are highly heterogeneous.

When comparing population exposure across SPI timescales of 1 (Figure 5), 3 (Figure S2), 6 (Figure S3), and 12 (Figure S4) months, no consistent pattern emerges. Table S1 presents comparisons of areal extent between Scale 1 vs. Scale 3, Scale 3 vs. Scale 6, and Scale 6 vs. Scale 12. Each cell (e.g., “1vs3”) summarizes the median, maximum, and the percentage of drought events in which the areal extent at the first scale (e.g., Scale 1) is greater than at the second scale (e.g., Scale 3). The supplementary table file provides a detailed explanation of how to interpret the tables. At shorter timescales, the maximum affected area is generally smaller, whereas the median areal extent is higher. This means that, for example, the maximum affected area across all events is smaller at Scale 1 compared to Scale 3, but the median affected area across all events is higher at Scale 1. The percentage of events with a larger median affected area at lower scales nonetheless varies considerably across continents and drought

https://doi.org/10.5194/essd-2025-646
Preprint. Discussion started: 3 February 2026

thresholds and for some parameter sets, the areal extent at longer timescales exceeds that at shorter timescales. For example, for a threshold of -2 and a buffer distance of 100 km, only 35.3% of the total events have a smaller affected area at SPI 3 compared to SPI 1. This occurs when regions not classified as drought-affected at shorter timescales are classified as drought-affected at longer timescales, because of drought conditions from preceding or subsequent months that are incorporated into the longer timescale calculation. We also find that at shorter timescales, droughts often correspond to lower severity values compared to longer timescales (Table S2). For example, in Europe at a 250 km buffer distance, 77.8% of drought events have higher severity at scale 12 compared to scale 6. Population exposure (Table S3) shows a clear relationship across scales: lower SPI timescales generally correspond to higher exposure values, reflecting their tendency to cover larger areas (Table S1). As area increases, population exposure typically increases as well. Nevertheless, a few cases show the opposite. This can be attributed to the highly uneven distribution of population, where a smaller area containing high population pixels may result in greater exposure than a larger but sparsely populated areas. Overall, our analysis highlights that the relationship between the different drought characteristics and between drought characteristics and population exposure presents some general patterns but is ultimately event-specific.

The SPEI results (Scale 1: Fig. 6; Scale 3: Fig. S5; Scale 6: Fig. S6; Scale 12: Fig. S7) show patterns broadly similar to those for SPI, except that Africa ranks second overall but moves to first at lower thresholds. Asia generally shows the highest population exposure across almost all thresholds and buffer distances, and shorter drought timescales often correspond to higher values in both areal extent (Table S4) and population exposure (Table S6), but lower severity levels (Table S5). Comparing SPI and SPEI in terms of areal extent (Table S7) at the same timescale, Africa and North America consistently show higher values for SPEI across all buffer distances. Regarding severity, SPEI typically identifies events as more severe than SPI (Table S8), with the exception of severity threshold -1, particularly in North America, South America, and Europe. Population exposure (Table S9) patterns mirror those of areal extent. SPI tends to identify lower population exposure in Asia and Africa, while in North America, South America and Europe, SPI often shows higher values than SPEI.

We next consider the weighted population exposure for SPI, which accounts for both drought severity and frequency. By definition, weighted exposure is smaller or equal to absolute exposure, as the weighting factors range between 0 and 1 (Sect. 3.4). The extent of the reduction in weighted exposure relative to absolute exposure provides insights into the nature of drought conditions. The largest reductions are observed in Asia, suggesting that droughts in this region may be less severe or less frequent within a given year than in other continents (Scale 1: Figure S8; Scale 3: Figure S9; Scale 6: Figure S10; Scale 12: Figure S11). Figures S12-S14 show both absolute and weighted population exposures at thresholds of -1, -1.5, and -2, respectively, for SPI scale 1. The degree of reduction again varies substantially across events and continents. North America, Africa and South America, in particular, show relatively smaller disparities between population exposure and weighted population exposure across thresholds, especially at a 500 km buffer distance. This disparity further diminishes across all continents as the buffer distance decreases, suggesting that at smaller distances, the algorithm captures more prolongued and severe drought events due to proximity to the target points. Figure S13 also suggests that disparity is usually greatest for events with higher absolute exposure, reinforcing

https://doi.org/10.5194/essd-2025-646
Preprint. Discussion started: 3 February 2026

the observation that widespread drought events are often associated with lower severity, shorter duration, or both. Similar observations are found at other scales (Figures S15–S23).

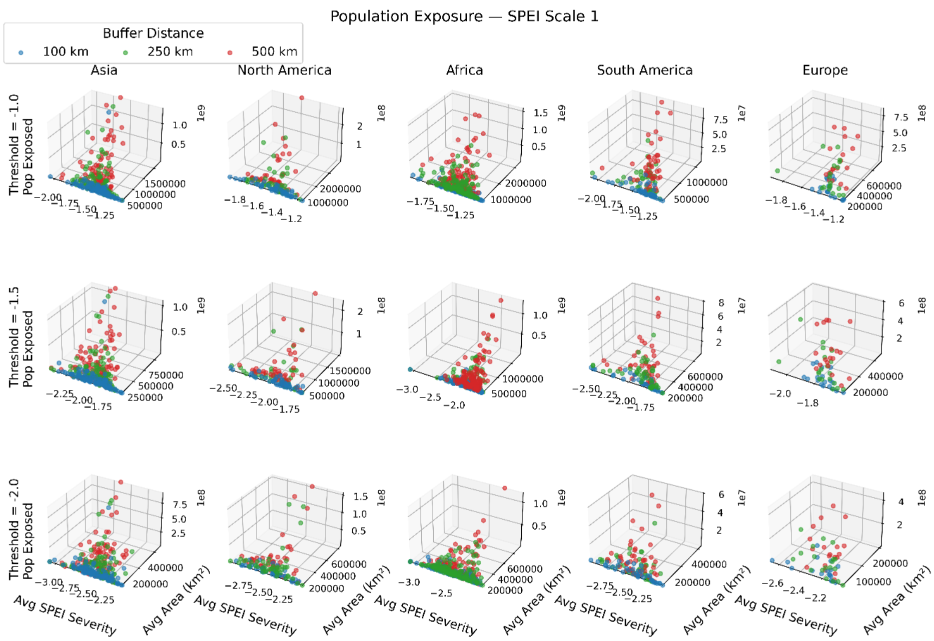

Figure 6. Population exposure to drought events based on SPEI-1 (1-month timescale) across five continents: Asia, North America, Africa, South America and Europe using the WSF population dataset.

In the weighted population estimates, the relative differences among continents are smaller than for absolute exposure. For example, at a 500-kilometer buffer distance, the variation across continents drops from a range of 650-60 million to 150-15 million. The relationships between exposure and drought characteristics, such as average areal extent (Table S10) and average severity (Table S11) across different temporal scales (Table S12) remain consistent with those observed for absolute population exposure.

The weighted population exposure based on SPEI shows the largest reductions in Asia, consistent with the pattern observed in SPI-based weighted exposure, particularly at buffer distances of 250 and 500 kilometers (Figures S24- S27). These reductions are more pronounced for drought events with higher absolute population exposure (Figures S28-S39). The relationships observed across different timescales in the SPEI-based weighted exposure are generally consistent with those seen in the unweighted SPEI population exposure data, except in some cases in Africa and South America (Tables S13-S15). Additionally, the relationship between weighted SPI and weighted SPEI population exposure closely mirrors that of the unweighted comparison (Tables S16-S18).

4.3) GDP Exposure Based on Gridded GDP

We next consider direct economic exposure to drought events in terms of GDP (Figure 7), again grouping results by continent. North America consistently exhibits the highest GDP

https://doi.org/10.5194/essd-2025-646
Preprint. Discussion started: 3 February 2026

exposure across all drought severity thresholds, as also reported by Gao et al. (2019). At a high buffer distance of 500 kilometers and threshold -1, GDP exposure reaches up to 15 trillion USD, primarily due to the concentration of high-value economic zones. Europe, Asia, and South America follow, with exposures ranging from approximately 1 to 10 trillion USD, while Africa reports about 0.4 trillion USD under the same buffer and severity values. This aligns with the findings of Sun et al. (2022), who observed that GDP exposure to droughts is highest in upper-middle-income countries and lowest in low-income, lower-middle-income, and low- to middle-income countries. Previous studies have also found that drought-affected GDP exposures usually exhibit similar patterns to population exposure and are highly correlated (O'Neill et al., 2014; Gu et al., 2020). However, in our analysis, population exposure and GDP exposure differ, reflecting the fact that pixel-level GDP exposure and population exposure values are not always well-correlated.

As the drought severity threshold becomes more severe, the areal extent of drought clusters and GDP exposure both decrease across all continents, a pattern similar to that observed for population exposure. When comparing GDP exposure across SPI timescales of 1, 3 (Figure S40), 6 (Figure S41), and 12 (Figure S42) months, drought characteristics show a mixed pattern. The changes in areal extent (Table S19) and severity (Table S20) across timescales closely resemble the median and maximum patterns observed for population exposure, with the differences being due to the different timeperiods over which the two analyses are conducted. The magnitude of these percentages is however generally lower compared to those for population exposure. Generally, as affected area increases, GDP exposure (Table S21) tends to rise accordingly, with few exceptions (cf. Table S19 and Table S21). These cases occur when a smaller area includes economically dense regions, resulting in higher GDP exposure than a larger area with low GDP.

The SPEI results (Scale 1: Figure 8; Scale 3: Figure S43; Scale 6: Figure S44; Scale 12: Figure S45) exhibit a broadly similar continental pattern to those observed for SPI. North America consistently shows the highest GDP exposure across all thresholds and buffer distances. This is followed by Asia, Europe, Africa and South America. When comparing drought characteristics across time scales, shorter timescales typically show a larger areal extent (Table S22) and higher GDP exposure (Table S24), but lower severity values (Table S23), which is consistent with the population exposure results. Compared to SPI data, a higher percentage of drought events show greater GDP exposure (Table S27) and larger areal extent (Table S25), along with more negative severity values (Table S26).

Weighted GDP exposure based on SPI has been computed for multiple scales (Scale 1: Figure S46; Scale 3: Figure S47; Scale 6: Figure S48; Scale 12: Figure S49), and comparative plots of weighted versus raw GDP exposure across various thresholds and scales are presented in Figures S50–S61. The degree of reduction from absolute to weighted GDP exposure varies by continent. Africa and South America, in particular, show comparatively small disparities between GDP and weighted GDP exposure across thresholds, especially at a 500 km buffer distance. This disparity further diminishes across all continents as the buffer distance decreases, mirroring the patterns observed in weighted population exposure. Notably, the extent of reduction is generally less pronounced in GDP exposure compared to population exposure. This difference may stem from the distribution of GDP values across grid cells, which for many droughts is more spatially uniform than population data. In such cases, a few high-density population pixels can significantly inflate exposure values, and when these are down-weighted,

https://doi.org/10.5194/essd-2025-646
Preprint. Discussion started: 3 February 2026

Open Access Earth System Science Data Discussions

it leads to a large decrease in exposure. Additionally, the relationship across timescales is similar for weighted GDP exposure (Table S30) compared to raw GDP exposure (Table S21). However, the number of events where GDP exposure is higher at shorter timescales than at longer ones decreases after weighting is applied.

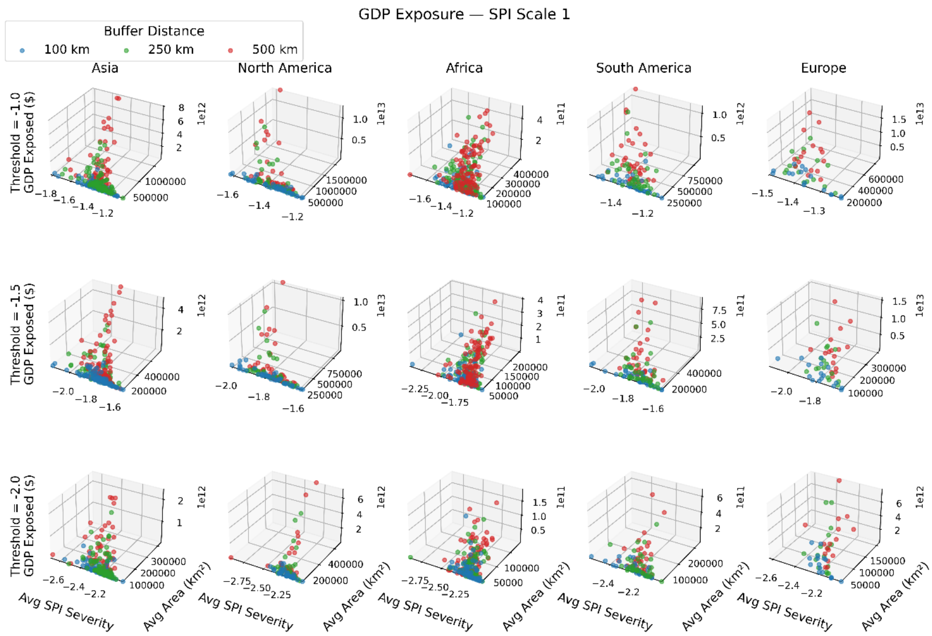

Figure 7. GDP exposure to drought events based on SPI-1 (1-month timescale) across five continents: Asia, North America, Africa, South America and Europe, using data from the global GDP dataset

The weighted GDP exposure (Scale 1: Figure S62; Scale 3: Figure S63; Scale 6: Figure S64; Scale 12: Figure S65) based on SPEI maintains the same continental ranking as the absolute GDP exposure. As for SPI, the reduction in GDP is more pronounced for events with higher raw GDP exposure (Figures S66-S77). Across timescales, a higher percentage of drought events exhibit greater GDP exposure at Shorter timescales, consistent with the pattern observed for absolute exposure (Table S34). However, the percentage decreases in a manner similar to the weighted GDP based on SPI. For the majority of events SPEI results in greater weighted GDP exposure than SPI, except for a few cases in Europe (Table S36).

https://doi.org/10.5194/essd-2025-646
Preprint. Discussion started: 3 February 2026

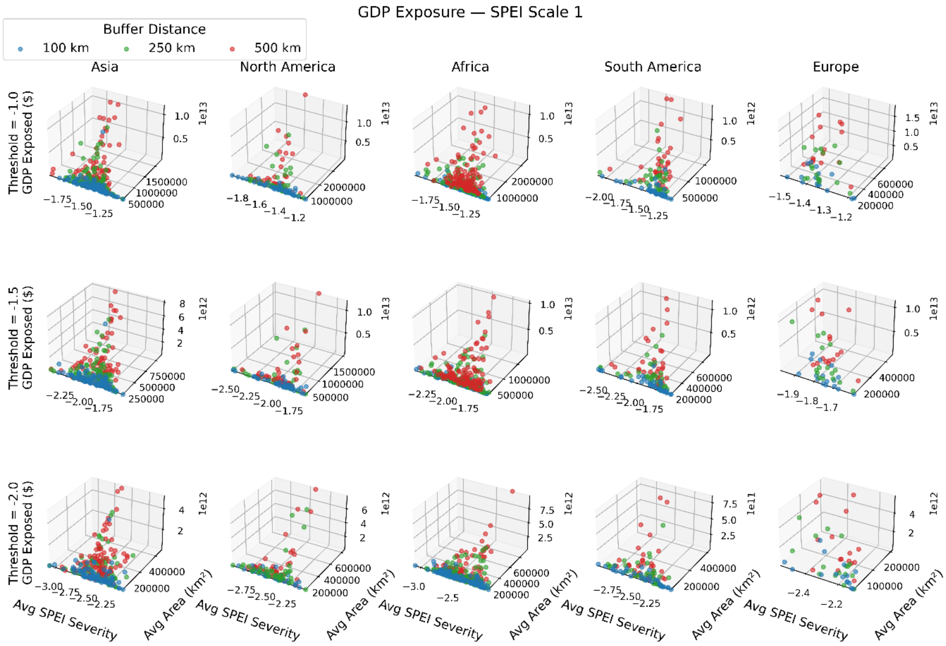

Figure 8. GDP exposure to drought events based on SPEI-1 (1-month timescale) across five continents: Asia, North America, Africa, South America and Europe, using data from the global GDP dataset

4.4) Population Impacted based on EM-DAT

We next examine drought impacts as reported in the EM DAT dataset. Figure 9 illustrates the number of persons affected for SPI-1 across four continents: Asia, North America, Africa and South America under three severity thresholds (-1, -1.5, -2) and buffer distances (100 km, 250 km, 500 km). Data for Europe and Australia are excluded due to small sample sizes. The affected population varies notably across continents. In Asia it reaches up to 200 million people, particularly at the 500 km buffer distance. Africa, South America and North America follow. This ranking is maintained across thresholds and scales. This contrasts with the exposure-based rankings, where North America shows higher population exposure than Africa and South America (Figure 1). However, both exposure and impact data consistently identify Asia as the most exposed and impacted continent. Interestingly, the affected population values remain nearly constant across thresholds and scales for each continent. This suggests that impacts are highly localised and associated with the gridpoints that satisfy the more stringent drought criteria. When examining drought area and severity across scales, often as the timescale increases (Figure S78-80), the magnitude of affected area (Table S37) decreases while drought severity (Table S38) increases.

https://doi.org/10.5194/essd-2025-646
Preprint. Discussion started: 3 February 2026

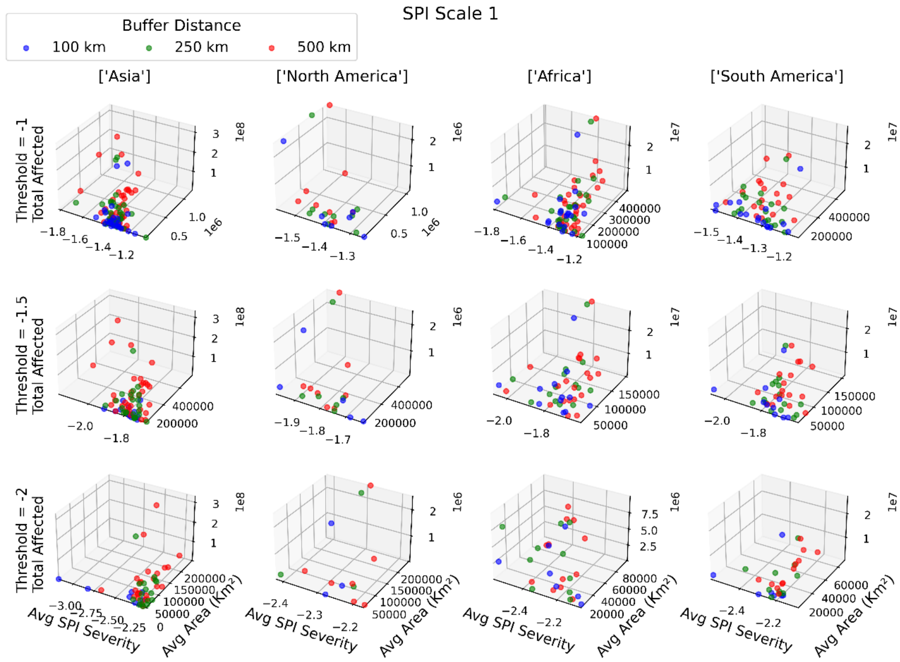

Figure 9. Population affected by drought events based on SPI-1 (1-month timescale) across four continents: Asia, North America, Africa, and South America, using data from the EM-DAT database.

Figures S12–S23 present event-level impact data (total affected) alongside both absolute and weighted population exposure estimates. Across different drought scales and thresholds, impact data generally co-varies with weighted exposure data, with few exceptions. In some cases, absolute exposure is smaller than the corresponding reported impact (Figure S94-S101). This is particularly evident in Asia (Figure S94), but isolated occurrences are also found in other continents. Indeed, Asia exhibits the weakest correlation between (weighted) exposure and impact among all continents (Figures S81–S82). Impact to exposure ratios above one indicate an inconsistency in the data sources that we use, either due to data errors or to discrepant definitions of drought. In fact, EM-DAT does not use physical indicators to define a disaster, but instead relies on its impacts and declarations of states of emergency.

SPEI captures larger affected populations, particularly in Asia, compared to SPI (Fig. 10), indicating that SPI may miss some high-impact events. Similar to the population exposure results, compared to SPI, SPEI shows a higher percentage of drought events with larger affected areas at shorter timescales (Table S39), while a lower percentage of events exhibit greater severity at shorter scales (Table S40). Because we use the same impact data for both drought indices, the relationship between SPI and SPEI for impacts remains similar to that observed for exposure (Tables S41–S42). Figures S29–S39 display event-level impact data alongside absolute and weighted population exposure estimates using SPEI. In Asia, several events again show impact-to-exposure rations above one (Figure S94). Nonetheless, in most cases impacts are lower than absolute exposure. Consequently, for SPEI the correlation between exposure and impact is higher than for SPI (Figure S82). This likely reflects the SPEI's broader detection of drought-affected areas, increasing exposure estimates.

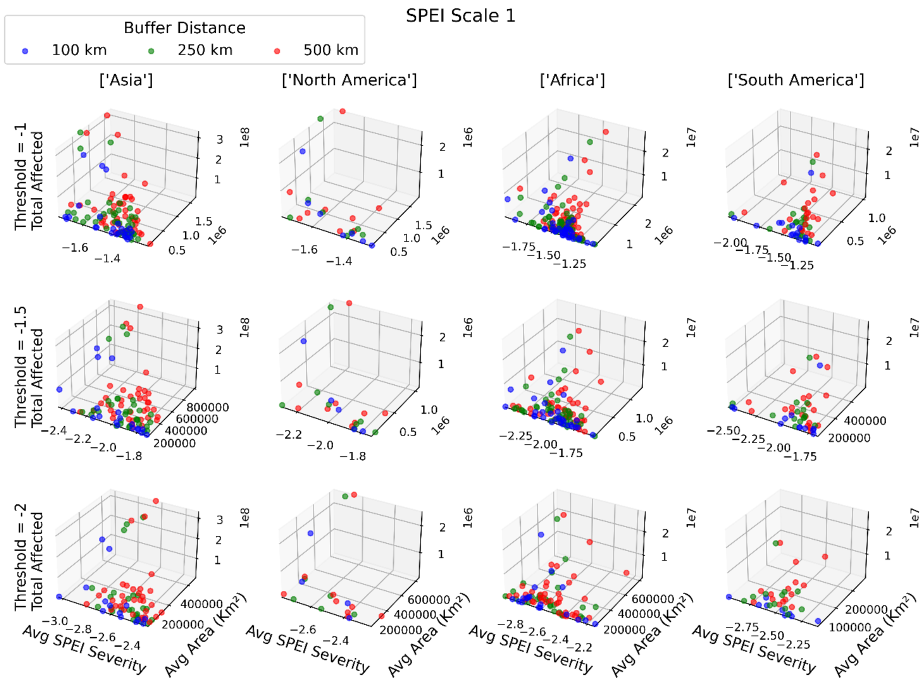

Figure 10. Population affected by drought events based on SPEI-1 (1-month scale) across four continents: Asia, North America, Africa, and South America, using data from the EM-DAT database.

4.5) Economic impact based on EMDAT

As a final step, we consider total economic damage in USD as recorded in the EM-DAT dataset across three continents: Asia, North America, and South America, at the SPI-1 (1-month) timescale (Figure 11). Africa, Europe, and Australia are excluded from the analysis due to limited economic damage data available in EM-DAT. At the -1 threshold, North America records the highest total damages, reaching up to 2.5 × 10^7 USD at a 500 km buffer distance, followed by Asia and South America. This same ranking is also observed in absolute and weighted GDP exposure. Total damage values remain nearly constant across thresholds and scales for each continent, with few exceptions, as the algorithm continues to register drought in grid cells associated with the highest economic impacts. Changes in economic damage across different scales, thresholds, and buffer distances are shown in Figures S86–S88.

Figures S50–S61 compare event-level impact data (total economic damage) with both absolute and weighted GDP exposure estimates using SPI. Across scales and thresholds, the damage data generally co-varies with the weighted exposure closely, except for a few high-GDP exposure events in Asia and North America which correspond to low economic impacts. There are no cases where the ratio of total damage to GDP exceeds one (Figure S102-S107).

https://doi.org/10.5194/essd-2025-646
Preprint. Discussion started: 3 February 2026

Open Access Earth System Science Data Discussions

Generally South America shows a higher correlation between (weighted) exposure and damage compared to Asia and North America (Figures S89–S90).

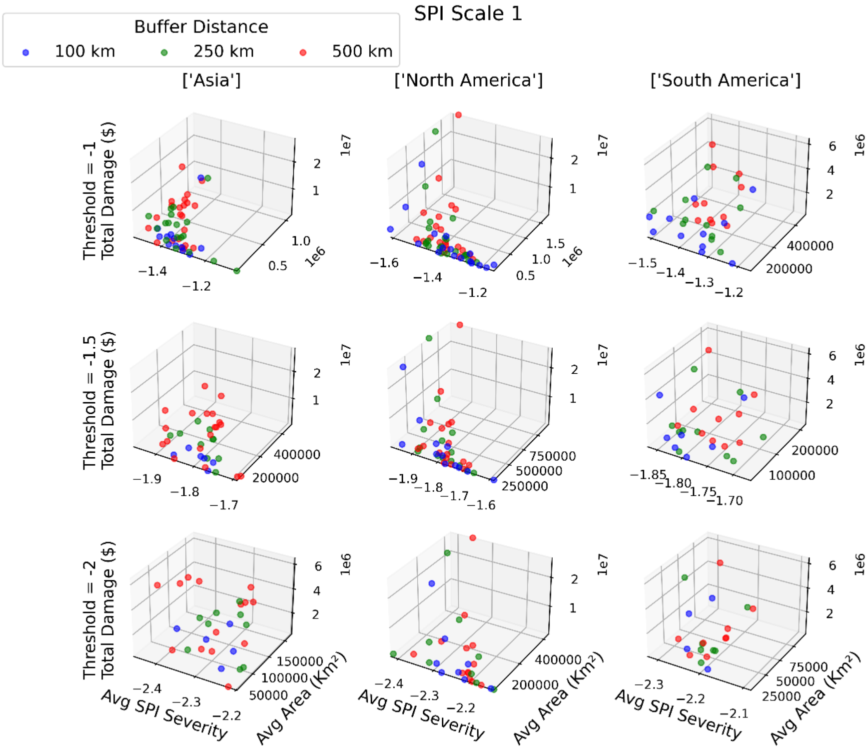

Figure 11. Total damage due to drought events based on SPI-1 (1-month timescale) across three continents: Asia, North America and South America, using data from the EM-DAT database.

Across all timescales, SPEI consistently corresponds to higher total economic damages from drought events than SPI. At the 1-month timescale (Figure 12), North America shows damage exceeding $\$2 \times 10^7$ USD, higher than equivalent SPI-based estimates, and Asia exhibits similar levels. SPEI preserves the same continental ranking as SPI across thresholds and scales (Figures S91-S93). The relationships among absolute GDP exposure, weighted GDP exposure, and total damage for SPEI remain consistent with the SPI-based patterns (Figures S66–S77). Overall, the correlation between (weighted) exposure and impact is found to be higher for SPEI than for SPI across all continents (Figures S89- S90).

https://doi.org/10.5194/essd-2025-646
Preprint. Discussion started: 3 February 2026

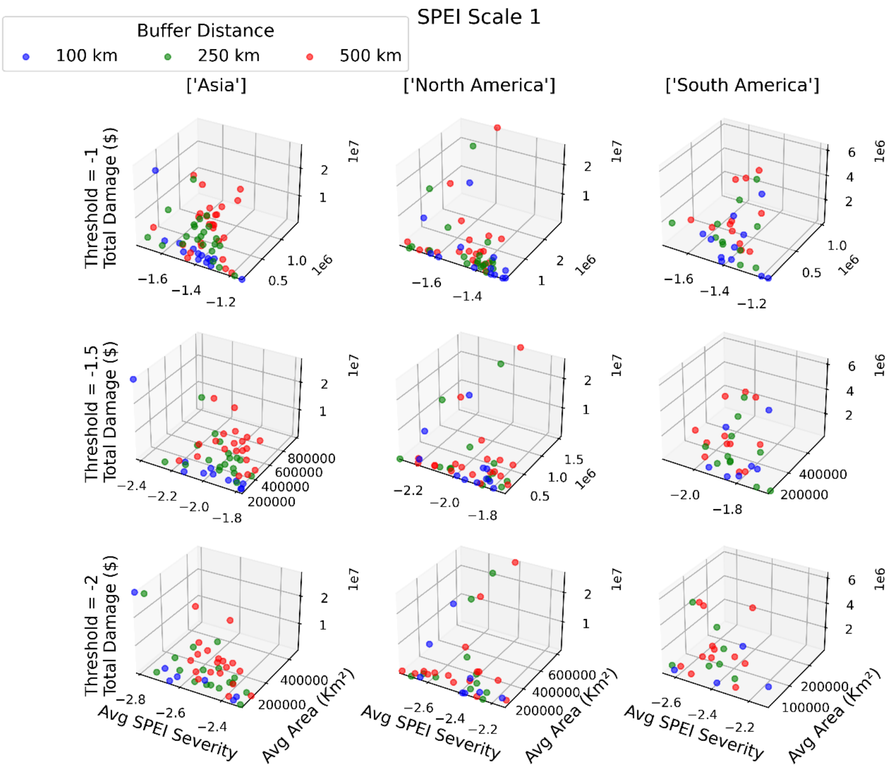

Figure 12. Total damage due to drought events based on SPEI-1 (1-month timescale) across three continents: Asia, North America and South America, using data from the EM-DAT database.

5) Data and code availability

The replication package (code, configuration files, derived outputs, and supplementary materials) is archived on Zenodo: https://doi.org/10.5281/zenodo.17251815. The record is currently restricted; editors and reviewers have access via a private link provided to the journal. Upon acceptance, the record will be made public under the same DOI.

Third-party source datasets:

- ERA5 climate reanalysis (precipitation, temperature; 0.25°): Copernicus Climate Data Store- https://cds.climate.copernicus.eu/
- GDIS (Geocoded Disasters): https://doi.org/10.7927/zz3b-8y61
- EM-DAT (Emergency Events Database): CRED- https://public.emdat.be/ (registration required; enable “Include historical events (pre-2000)”)
- Global GDP (1990–2022, 5-arcmin GeoTIFF): Kummu et al. (2023); Zenodo: https://zenodo.org/records/13943886
- WSF Population Time Series (1975–2025): Marconcini et al., 2020; Zenodo: https://zenodo.org/records/13943886

https://doi.org/10.5194/essd-2025-646
Preprint. Discussion started: 3 February 2026

6) Conclusions

This study presents a comprehensive analysis of global drought exposure and impacts using an integrated framework that combines meteorological drought indices (SPI and SPEI), spatial clustering techniques, and data on population, GDP, affected people and economic damage. By examining multiple drought timescales (1, 3, 6, and 12 months) and thresholds (-1, -1.5, and -2) and applying various buffer distances (100 km, 250 km, and 500 km) to connect droughts to their impacts, the methodology captures the evolution and spatial footprint of drought events and integrates them with exposure and impacts. We view this as a key step towards planning and risk mitigation for droughts.

We highlight that the impact analyses in this study are based on the EM-DAT and GDIS databases, and are therefore subject to the datasets' reporting biases. As EM-DAT relies on national and international disaster reporting mechanisms, underreporting or inconsistencies may affect the completeness and accuracy of the recorded drought impacts. Consequently, interpretation of the results should be undertaken with caution, and findings should be considered within the context of potential data limitations.

Our key conclusions are as follows:

- The sensitivity analysis shows that the proportion of drought events recorded in GDIS for which drought clusters have been detected, decreases with increasing scale, decreasing buffer distance, and more stringent thresholds for both SPI and SPEI. Additionally, for a given threshold, buffer distance, and timescale, detection percentages are consistently higher for SPEI than for SPI.
- No consistent relationship between drought characteristics (such as severity or area) and drought timescale emerges for either SPI or SPEI.
- Asia shows the highest population exposure across almost all the scales and thresholds, for both the SPI and SPEI indices. North America shows the highest GDP exposure across nearly all drought timescales and thresholds, for both the SPI and SPEI indices.
- SPEI-based droughts generally cover larger areas than SPI-based droughts, resulting in greater population and GDP exposures
- No consistent relationship is observed when comparing GDP and population exposure across different timescales. However, for the majority of events, both population exposure and weighted population exposure, as well as GDP exposure and weighted GDP exposure, decrease with increasing timescale and more stringent thresholds.
- Asia and North America show the highest numbers of people affected and the greatest total damage for both SPI and SPEI, respectively, in line with the fact that they also show the highest exposures. These impacts remain consistently large across different drought timescales and severity thresholds, indicating that the highest-impact events are long-lasting and particularly severe droughts.
- The correlation between (weighted) population exposure and total affected, varies across continents and is lowest in Asia. In Asia, the total affected population is sometimes higher than the exposed population, pointing to inconsistencies in the data used here.
- Similarly, the correlation between (weighted) GDP exposure and total damage, varies across continents. However, unlike total affected, total damage rarely exceeds absolute GDP exposure for the events considered.

616 This study highlights the varied physical characteristics of drought and exposure and impacts of drought across different continents. It further elucidates the sensitivity to the choice of indices, timescales, and severity thresholds used to define drought. Integrating physical drought indicators with socio-economic exposure and impact data can significantly improve drought risk planning and mitigation efforts.

621 **Author contributions**

622 **AS**: Conceptualization (equal); Data curation (lead); Formal analysis (lead); Methodology (lead); Visualization (lead); Writing – original draft preparation (lead); Writing – review & editing (lead). **GM**: Conceptualization (equal); Funding Acquisition (lead); Methodology (supporting); Writing – review & editing (supporting).

626 **Competing interests**

627 The contact author has declared that none of the authors has any competing interests.

628 **Acknowledgements**

629 We acknowledge the financial support received from the European Research Council (ERC) under the European Union's Horizon 2020 and Horizon Europe research and innovation programmes (Grants 948309, "CENÆ" and 101112727, "ICE-MOT") and from the Swedish Research Council Vetenskapsrådet (proj. no. 2022-03448 and 2022-06599.)

633 **References**

634 AghaKouchak, A., Huning, L. S., Sadegh, M., Qin, Y., Markonis, Y., Vahedifard, F., ... & Kreibich, H.: Toward impact-based monitoring of drought and its cascading hazards. Nature Reviews Earth & Environment, 4(8), 582-595, 2023.

637 Bevacqua, E., Rakovec, O., Schumacher, D. L., Kumar, R., Thober, S., Samaniego, L., ... & Zscheischler, J.: Direct and lagged climate change effects intensified the 2022 European drought. Nature Geoscience, 1-8, 2024.

640 Buras, A., Rammig, A., & Zang, C. S.: Quantifying impacts of the 2018 drought on European ecosystems in comparison to 2003. Biogeosciences, 17(6), 1655-1672, 2020.

642 Ceola, S., Mård, J., & Di Baldassarre, G.: Drought and human mobility in Africa. Earth's Future, 11(12), e2023EF003510, 2023.

644 Chen, B., Wu, S., Jin, Y., Song, Y., Wu, C., Venevsky, S., ... & Gong, P.: Wildfire risk for global wildland–urban interface areas. Nature Sustainability, 7(4), 474-484, 2024.

646 Cook, B. I., Mankin, J. S., Marvel, K., Williams, A. P., Smerdon, J. E., & Anchukaitis, K. J.: Twenty-first century drought projections in the CMIP6 forcing scenarios. Earth's Future, 8(6), e2019EF001461, 2020.

649 Ghasempour, R., Roushangar, K., Ozgur Kirca, V. S., & Demirel, M. C.: Analysis of spatiotemporal variations of drought and its correlations with remote sensing-based indices via wavelet analysis and clustering methods. Hydrology Research, 53(1), 175-192, 2022.

652 Gu, L., Chen, J., Yin, J., Sullivan, S. C., Wang, H. M., Guo, S., ... & Kim, J. S.: Projected increases in magnitude and socioeconomic exposure of global droughts in 1.5 and 2 C warmer climates. Hydrology and Earth System Sciences, 24(1), 451-472, 2020.

Guha-Sapir, D., Below, R., & Hoyois, P.: EM-DAT: The International Disaster Database. Centre for Research on the Epidemiology of Disasters (CRED). Retrieved from: https://www.emdat.be, 2023.

Herrera-Estrada, J. E., Satoh, Y., & Sheffield, J.: Spatiotemporal dynamics of global drought. Geophysical Research Letters, 44(5), 2254-2263, 2017.

Hersbach, H., Bell, B., Berrisford, P., Biavati, G., Horányi, A., Muñoz Sabater, J., Nicolas, J., Peubey, C., Radu, R., Rozum, I., Schepers, D., Simmons, A., Soci, C., Dee, D., Thépaut, J-N. : ERA5 hourly data on single levels from 1940 to present. Copernicus Climate Change Service (C3S) Climate Data Store (CDS), doi: 10.24381/cds.adbb2d47 (Accessed on 19-08-2024), 2023.

Jägermeyr, J., & Frieler, K.: Spatial variations in crop growing seasons pivotal to reproduce global fluctuations in maize and wheat yields. Science Advances, 4(11), eaat4517, 2018.

Kafle, H., Khaitu, S., Gyawali, D., Shrestha, D., Koirala, D., Kamaruzzaman, M., ... & Yamaguchi, Y.: Historical drought and its trend in South Asia: Spatial and temporal analysis 2000-2020. APN Science Bulletin, 12(1), 190 – 204. doi: 10.30852/sb.2022.2022, 2022.

Kageyama, Y., & Sawada, Y.: Global assessment of subnational drought impact based on the Geocoded Disasters dataset and land reanalysis. Hydrology and Earth System Sciences, 26(18), 4707-4720, 2022.

Khan, M. M. H., Muhammad, N. S., & El-Shafie, A.: A review of fundamental drought concepts, impacts and analyses of indices in Asian continent. Journal of Urban and Environmental Engineering, 12(1), 106-119, 2018.

Kulkarni, S., Sawada, Y., Bayissa, Y., & Wardlow, B.: Global Assessment of Socio-Economic Impacts of Subnational Droughts: A Comparative Analysis of Combined Versus Single Drought Indicators. Hydrology and Earth System Sciences Discussions, 2024, 1-35, 2024.

Kumar, K. S., AnandRaj, P., Sreelatha, K., & Sridhar, V.: Regional analysis of drought severity-duration-frequency and severity-area-frequency curves in the Godavari River Basin, India, 2021.

Kummu, M., Kosonen, M. & Masoumzadeh Sayyar, S.: Downscaled gridded global dataset for gross domestic product (GDP) per capita PPP over 1990–2022. Scientific Data 12: 178. https://doi.org/10.1038/s41597-025-04487-x, 2025.

Marconcini, M., Metz-Marconcini, A., Üreyen, S., Palacios-Lopez, D., Hanke, W., Bachofer, F., ... & Strano, E.: Outlining where humans live, the World Settlement Footprint 2015. Scientific Data, 7(1), 242, 2020.

Marengo, J. , Cunha, A. , Espinoza, J. , Fu, R. , Schöngart, J. , Jimenez, J. , Costa, M. , Ribeiro, J. , Wongchuig, S. & Zhao, S.: The Drought of Amazonia in 2023-2024. American Journal of Climate Change, 13, 567-597. doi: 10.4236/ajcc.2024.133026, 2024.

Marengo, J. A., Galdos, M. V., Challinor, A., Cunha, A. P., Marin, F. R., Vianna, M. D. S., Alvala, R.C., Alves, L.M., Moraes, O.L. & Bender, F.: Drought in Northeast Brazil: A review of agricultural and policy adaptation options for food security. Climate Resilience and Sustainability, 1(1), e17, 2022.

McKee, T. B., Doesken, N. J., & Kleist, J.: The relationship of drought frequency and duration to time scales. In Proceedings of the 8th Conference on Applied Climatology, 17, 22, 179-183, 1993.

Mishra, A. K., & Singh, V. P.: Analysis of drought severity-area-frequency curves using a general circulation model and scenario uncertainty. Journal of Geophysical Research: Atmospheres, 114(D6), 2009.

Mishra, A. K., & Singh, V. P.: A review of drought concepts. Journal of hydrology, 391(1-2), 202-216, 2010.

Mishra, A. K., & Singh, V. P.: Drought modeling–A review. Journal of Hydrology, 403(1-2), 157-175, 2011.

Mondal, S. K., Huang, J., Wang, Y., Su, B., Zhai, J., Tao, H., ... & Jiang, T.: Doubling of the population exposed to drought over South Asia: CMIP6 multi-model-based analysis. Science of the Total Environment, 771, 145186, 2021.

O'Neill, B. C., Kriegler, E., Riahi, K., Ebi, K. L., Hallegatte, S., Carter, T. R., ... & Van Vuuren, D. P.: A new scenario framework for climate change research: the concept of shared socioeconomic pathways. Climatic change, 122(3), 387-400, 2014.

Penalba, O. & Rivera, J.: Future Changes in Drought Characteristics over Southern South America Projected by a CMIP5 Multi-Model Ensemble. American Journal of Climate Change, 2, 173-182. doi: 10.4236/ajcc.2013.23017, 2013.

Petersen-Perlman, J. D., Aguilar-Barajas, I., & Megdal, S. B.: Drought and groundwater management: Interconnections, challenges, and policyresponses. Current Opinion in Environmental Science & Health, 28, 100364, 2022.

Pokhrel, Y., Felfelani, F., Satoh, Y., Boulange, J., Burek, P., Gädeke, A., ... & Wada, Y.: Global terrestrial water storage and drought severity under climate change. Nature Climate Change, 11(3), 226-233, 2021.

Rosvold, E., & Buhaug, H.: Geocoded Disasters (GDIS) Dataset (Version 1.00) [Data set]. Palisades, NY: NASA Socioeconomic Data and Applications Center (SEDAC). https://doi.org/10.7927/ZZ3B-8Y61, 2021.

Samantaray, A. K., Ramadas, M., & Panda, R. K.: Changes in drought characteristics based on rainfall pattern drought index and the CMIP6 multi-model ensemble. Agricultural Water Management, 266, 107568, 2022.

Samantaray, A. K., Ramadas, M., Babbar-Sebens, M., & Gautam, S.: Assessment of Nonstationary Drought Frequency under Climate Change Using Copula and Bayesian Hierarchical Models. Journal of Hydrologic Engineering, 30(2), 04025002, 2025.

Samantaray, A. K., & Messori, G.: Reproducible Workflows for Global Drought Clustering with Socioeconomic Exposure (v1.0.0), https://doi.org/10.5281/zenodo.17251815, 2025.

Sun, F., Wang, T., & Wang, H.: Mapping Global GDP Exposure to Drought. In Atlas of Global Change Risk of Population and Economic Systems (pp. 123-130). Singapore: Springer Nature Singapore, 2022.

https://doi.org/10.5194/essd-2025-646
Preprint. Discussion started: 3 February 2026

Tsakiris, G., Loukas, A., Pangalou, D., Vangelis, H., Tigkas, D., Rossi, G., & Cancelliere, A. : Drought characterization. Drought management guidelines technical annex, 58, 85-102, 2007.

UNCCD.: Global drought snapshot 2023. https://shorturl.at/YQSte, 2023.

Vicente-Serrano, S. M., Beguería, S., & López-Moreno, J. I.: A multiscalar drought index sensitive to global warming: the standardized precipitation evapotranspiration index. Journal of climate, 23(7), 1696-1718, 2010.

Vicente-Serrano, S. M., Peña-Angulo, D., Beguería, S., Domínguez-Castro, F., Tomás-Burguera, M., Noguera, I., ... & El Kenawy, A.: Global drought trends and future projections. Philosophical Transactions of the Royal Society A, 380(2238), 20210285, 2022.

Wilhite, D. A.: Drought as a natural hazard: concepts and definitions. In Droughts (pp. 3-18). Routledge, 2016.

Yevjevich, V. M.: An objective approach to definitions and investigations of continental hydrologic droughts (Vol. 23, p. 25). Fort Collins, CO, USA: Colorado State University, 1967.

Zarch, M. A. A., Sivakumar, B., & Sharma, A.: Droughts in a warming climate: A global assessment of Standardized precipitation index (SPI) and Reconnaissance drought index (RDI). Journal of hydrology, 526, 183-195, 2015.

Zargar, A., Sadiq, R., Naser, B., & Khan, F. I.: A review of drought indices. Environmental Reviews, 19(NA), 333-349, 2011.

Zhang, R., Shangguan, W., Liu, J., Dong, W., & Wu, D.: Assessing meteorological and agricultural drought characteristics and drought propagation in Guangdong, China. Journal of Hydrology: Regional Studies, 51, 101611, 2024.